
Article:
Yang, H., Lyu, S., Zhu, Z.Q. et al. (2018) Novel dual-stator machines with biased permanent magnet excitation. IEEE Transactions on Energy Conversion, 33 (4). pp. 2070-2080. ISSN: 0885-8969

https://doi.org/10.1109/TEC.2018.2866464

Novel Dual Stator Machines with Biased Permanent Magnet Excitation

Hui Yang, *Member, IEEE*, Shukang Lyu, Z. Q. Zhu, *Fellow, IEEE*, Heyun Lin, *Senior Member, IEEE,* S. S. Wang, Shuhua Fang, and Yunkai Huang

***Abstract*—This paper proposes high-torque-density dual stator permanent magnet machines with biased permanent magnet (PM) excitation in the inner stator. The developed machine can be geometrically considered as an outer-rotor stator PM machine plus a separate outer stator similar to the conventional fractional-slot machines. Consequently, the proposed designs feature two different stator structures. Meanwhile, two sets of armature windings are employed to improve the space utilization ratio and torque density. The machine topologies and operating principles are first described. In addition, the analytical models of the machine are introduced, which are utilized to optimize the stator/rotor pole combination as well as the power splitting ratio between two stators. This design optimization is performed in order to maximize the torque capability with the constraint of copper loss. The electromagnetic characteristics of the proposed machine with different inner stator structures are evaluated and compared by the finite-element (FE) method. Finally, an optimized DS-BPMM prototype is manufactured and tested to verify the FE analyses.**

***Index Terms*—Biased flux; dual stator; permanent magnet (PM) machine, partitioned stator, switched flux.**

I. INTRODUCTION

DUE TO the advantages of high torque density, high efficiency and convenient maintenance, permanent magnet (PM) machines have been widely utilized in various industry applications, such as electric vehicle (EV), vessel propulsion, domestic appliances, and wind power generation [1]-[3]. However, the demands of high torque/power rating in these applications usually make those conventional PM machines suffer from bulky size and large material consumption [2]. Thus, the torque density improvement is extensively recognized as a challenging issue for the traditional PM machines. Therefore, many researchers attempted to find utility methods for torque density enhancement for PM machines. As a common practice, doubling the stator [4] [5] or rotor [6]-[20], namely, dual-mechanical-port machine [4], is normally employed to increase the torque density within limited overall dimension. The dual rotor (DR) machines usually require sophisticated efforts for handling two rotating parts, which leads to relatively low mechanical reliability. The dual stator (DS) machine was relatively structurally simpler by using an additional stator as a torque booster, and better control flexibility can be achieved [4].

Accordingly to the PM position, the DS machines [7]-[20] can be generally categorized as rotor-PM [7]-[12] and stator-PM [13]-[21] topologies. For the rotor-PM machines [7]-[12], the thermal management and protection issues associated with the PMs tend to be problematic issues for the DS machine with cantilever cupped rotor. On the other hand, the stator-PM DS [13]-[19] machine can well facilitate the PM heat dissipation, but also have simple and robust rotor which is preferable for high-speed critical-safety operation.

The switched flux (SF) [13]-[19] and doubly salient [20] designs were extended to the DS structures in potential context of automotive traction applications. In general, the stator-PM DS machines can be divided into yoke [13]-[14] and yokeless [15]-[19] types based on the rotor structure. The former type can be considered as a combination of two identical single-stator SFPM machines [14]. Meanwhile, the magnetic circuits of two sub-machines are electromagnetically decoupled. In [14], the possibility of SF DS machine as a "dual-mechanical-port" option for extended-range EV was discussed. In this case, the inner SFPM machine works as a generator to charge the batteries, which offer additional energy to the outer SFPM machine to drive the vehicle. On the other hand, the yokeless rotor, i.e., segmental rotor structure is employed for another type of DS SFPM machines, which shows advantageous structural compactness. The PMs that are directly opposite to each other in both stators must be of reverse polarity. The yokeless SF DS machine is geometrically similar to that of magnetically geared machines [11]. In terms of the operating principle, the yokeless DS design can be recognized as a combination of a magnetic gear and an electrical machine within one frame having two stationary parts and one rotating rotor segments [15] [16]. The multiple air-gap field harmonics are involved into effective torque production. However, the magnetic circuits of PMs on the inner and outer stators are series, and significant magnetic saturation can be induced, which is undesirable for the torque improvement. In order to alleviate this problem, an alternate ferrite design was presented to maintain comparable torque density with the conventional interior-PM (IPM) machine while maintaining the advantage of low cost [19]. Nevertheless, as the inner and outer stators are structurally duplicated, the geometric conflicts between the PM excitations and windings on the stator still exist in those single stator counterparts [15] [16]. This causes the reduction of the slot area for accommodating armature windings when the air-gap diameter is fixed. Hence, the torque density may be still compromised.

Therefore, this paper aims to propose novel DS biased PM machines (DS-BPMM) only having PM excitations in the inner stators. Different from the existing DS machines [15] [16]

having two identical stator configurations, the developed DS-BPMMs combines the advantages of the design concept of "partitioned stator (PS)" [17]-[19] and conventional DS machines [15]-[17]. In the perspective of the geometry, the proposed machine can be considered as a synergy of an outer-rotor stator PM machine plus a separate outer stator similar to the conventional fractional-slot machines [15]. As a result, the space tradeoff between PM and copper areas can be significantly alleviated compared to traditional DS counterparts as aforementioned.

The paper is organized as follows. The topology evolution and operating principle of the DS-BPMM are introduced in Section II. Section III is devoted to the analytical modeling of the developed machine. In Section IV, the power splitting ratio between two stators and the stator/rotor pole combination are analytically optimized in order to maximize torque capability with the constraint copper loss. The electromagnetic characteristics of the proposed machine with different DS structures are evaluated and compared by the finite-element (FE) method in Section V. In Section VI, an optimized DS-BPMM prototype is manufactured and tested to verify the FE analyses.

II. Topology Evolution and Operating Principle

A. Machine Topologies

Fig. 1(a) shows typical configuration of a 6/11-stator slot/rotor pole DS-BPMM with a spoke-type inner stator. The proposed DS-BPMM can be geometrically considered an outer rotor SFPM machine and a separate outer stator. The three-phase non-overlapping tooth-coil windings are employed in two stators, which take the advantages of short end-windings and easy manufacture, and high efficiency. The outer stator serves as a prime armature field excitation, while the inner stator employs a secondary armature winding for the torque generation. In addition, the rotor segments are sandwiched between the two stators, which are structurally similar to a magnetically geared machine [11].

The topology of the proposed DS-BPMM can be derived from a conventional PS machine as shown in Fig. 1(b) by replacing the cylindrical solid inner stator with a salient-pole inner stator having "U"-shaped iron core. In this case, the total iron material will be reduced by approximately 40%, and then a secondary armature winding is employed within the inner stator so as to improve the space utilization ratio. Thus, the proposed DS-BPMM also benefits from the alleviation of geometric conflict between the magnetic and electric loadings in PS structure. Meanwhile, the torque density can be further improved with significantly reduced PM usage compared to the existing DS counterparts [8]-[16], making the developed machine beneficially cost-effective.

The torque/current characteristics of the PS and DS machines are plotted in Fig. 2. It can be seen that the proposed DS BPMM even shows comparable average torque with only outer winding with the PS one. Meanwhile, the developed DS machine can provide ~36.6% higher torque capability than the PS counterpart with an additional inner stator. Thus, the torque improvement of the proposed DS design over the PS machine is confirmed.

B. Operating Principle

The operating principle of the proposed machine can be physically understood by two perspectives. Firstly, it is basically an outer rotor SFPM machine, and the alignment or misalignment between rotor segments allows switched flux action, i.e., the basically sinusoidal and bipolar coil flux linkage will be induced as illustrated in Fig. 3. In addition, from the viewpoint of "magnetic gearing concept", the machine can be considered as a magnetically geared machine [11] consisting of two stationary parts and a sandwiched rotor.

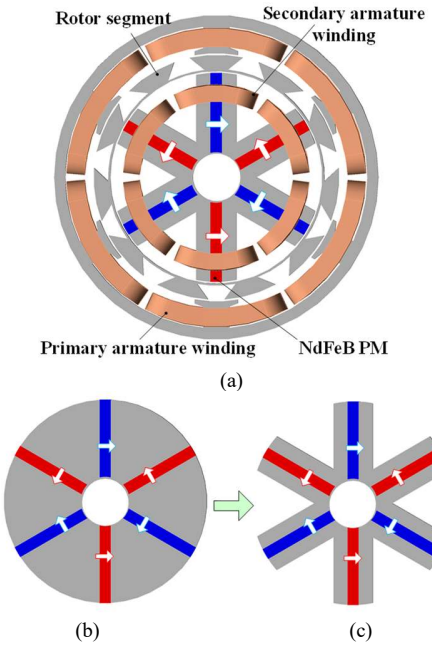

Fig. 1. (a) The proposed DS-BPMM configuration. (b) Cylinder inner stator: partitioned stator. (c) "V"-shaped salient stator design.

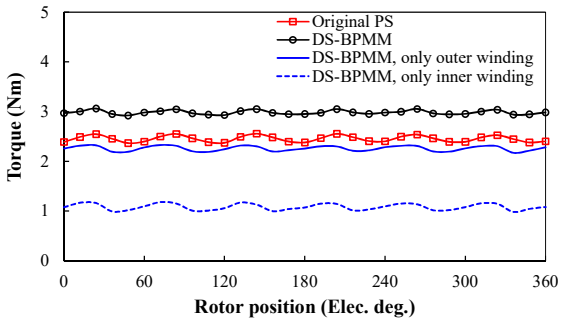

Fig. 2. Comparison of steady torque waveforms of the original PS machine and proposed DS-BPMM, rated current=10Arms.

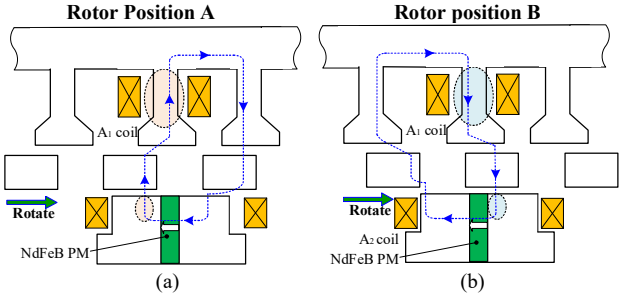

Fig. 3. The operating principle of the proposed DS-BPMM. (a) Rotor position A. (c) Rotor position B.

III. Analytical Design Procedure for Torque Density Maximization

Since there are multiple parameters in the DS-BPMM, it is necessary to develop a simple and computationally efficient analytical design procedure to facilitate the preliminary design. Fig. 4 illustrates the simplified sketch of the proposed design labelled with the key design parameters. Obviously, the inner slot-opening width is greatly affected by the magnet thickness, and hence β_{ms}, i.e., the ratio of inner slot-opening width τ_{so} to NdFeB PM width τ_m, is significant for balancing the magnetic and electric loading since the PM excitations are placed in the inner stator, which can be expressed as

$$\beta_{\mathrm{ms}} = \tau_{so} / \tau_m \tag{1}$$

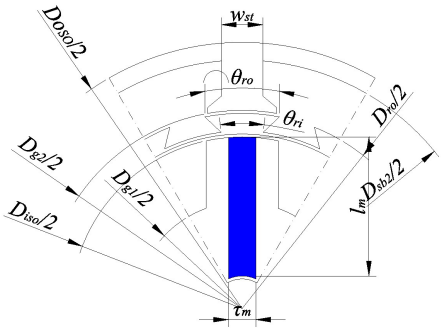

Fig. 4. Illustration of the design parameters in DS-BPMM.

Firstly, the power splitting ratio $k_{pow.}$ between two separate stators should be considered in advance, which can be expressed as

$$k_{pow.} = \frac{P_o}{P_i} \tag{2}$$

where P_o and P_i are the electromagnetic powers delivered by the interaction between two individual sets of windings and PMs, under zero d-axis current control, which can be given by

$$P_o = 3E_{oa}I_{oa}\eta = \sqrt{2}\pi\eta k_w L_a D_{g2}^2 A_o B_{o\delta}\omega_r / 4 \tag{3a}$$

$$P_i = 3E_{ia}I_{ia}\eta = \sqrt{2}\pi\eta k_w L_a D_{g1}^2 A_i B_{i\delta}\omega_r / 4 \tag{3b}$$

where E_{ia}/E_{oa} and I_{ia}/I_{oa} are the root-mean-square (RMS) value of fundamental no-load phase back-EMF and RMS phase current of the inner/outer windings, ω_r is the mechanical angular speed (rad/s), D_{g1} and D_{g2} are the outer diameter of the inner stator and the inner diameter of the outer stator, respectively, L_a is the effective stack length, η is the efficiency, $B_{o\delta}$ and $B_{i\delta}$ are the maximum air-gap flux density, A_i/A_o are the inner/outer electric loadings, and k_w is the winding factor. Dividing (3a) by (3b), the power splitting ratio can be rewritten as

$$k_{pow.} = \frac{P_o}{P_i} = \frac{A_o D_{g2}^2}{A_i D_{g1}^2} \tag{4}$$

where the electric loadings regarding inner and outer air-gaps can be expressed as

$$A_i = \frac{6k_p J_{si} A_{si}}{\pi D_{g2}} \tag{5a}$$

$$A_o = \frac{6k_p J_{so} A_{so}}{\pi D_{g1}} \tag{5b}$$

where k_p is the slot packing factor, J_{si}/J_{so} is the inner/outer current density, N_{si}/N_{so} are the numbers of inner/outer stator slots, A_{si}/A_{so} are the inner and outer armature copper areas per slot. On the other hand, the turns per phase in inner and outer windings can be governed by

$$J_{si}A_{si}k_p = N_{ia}I_{ia} \tag{6a}$$

$$J_{so}A_{so}k_p = N_{oa}I_{oa} \tag{6b}$$

During the optimization process, the armature current density and total copper loss P_{copper} are fixed as 6.5A/mm^2 and 40W, respectively, and hence the following constraint can be obtained, i.e.

$$P_{copper} = \rho L_a N_s \frac{(N_{ia}I_{ia})^2}{k_p A_{si}} + \rho L_a N_s \frac{(N_{oa}I_{oa})^2}{k_p A_{so}} = Const. \tag{7}$$

where ρ is the resistivity of copper wire, N_s is the stator slot number. Thus, it can be deduced from the above formula that the power/torque density are predominantly sensitive to β_{ms} and an effective split ratio λ_s defined as

$$\lambda_s = D_{g1} / D_{g2} \tag{8}$$

A. Simplified Analytical Model

In order to optimize the power splitting ratio, a simplified analytical model as illustrated in Fig. 5 is established to calculate the air-gap flux density distributions and electromagnetic torque based on magneto-motive-force (MMF)-permeance theory. In this model, the permeability of iron core is assumed to be infinite, and magnetic saturation is neglected. Besides, the analytical model is regarded as a 2-D problem, and no end-effects are considered. As a result, the open-circuit air-gap flux density can be rapidly obtained by multiplying stationary PM MMF and air-gap permeance formed by stator/rotor doubly saliency structure.

1) PM MMF

By ignoring the high-order harmonics, PM MMF can be formatted as [21] [22]

$$F_m = \sum_{i=1,3,5...}^{\infty} F_i \cos\left(\frac{iN_s\theta_s}{2}\right) \approx F_1 \cos\left(\frac{N_s}{2}\theta_s\right) + F_3 \cos\left(\frac{3N_s}{2}\theta_s\right) \tag{9}$$

where the fundamental and third harmonics of PM MMF F_1 and F_3 can be given by

$$F_1 \approx \frac{4}{\pi} \frac{k_{\alpha 1} B_r h_m}{\mu_0 \mu_r \left(2 + \frac{h_m}{g k_{cs} k_{cr}} \frac{\tau}{\tau_m}\right)} \tag{10a}$$

$$F_3 \approx \frac{4}{3\pi} \frac{k_{\alpha 3} B_r h_m}{\mu_0 \mu_r \left(2 + \frac{h_m}{g k_{cs} k_{cr}} \frac{\tau}{\tau_m}\right)} \tag{10b}$$

where F_i is ith harmonic of PM MMF, B_r is the PM remanence flux density, θ_s is relative position of stator and rotor teeth, h_m is PM thickness, l_m is the magnet length, τ is the pole pitch. $k_{\alpha 1}$ and $k_{\alpha 3}$ are the pole-arc coefficients corresponding to the fundamental and third harmonics of PM MMF. k_{cs} and k_{cr} are the rotor and stator Carter factor.

2) Air-Gap Permeance

The air-gap permeances due to slotted stator/rotor saliency can be given by

$$\Lambda_s(\theta_s)=\frac{\mu_0}{g+\delta(\theta_s)} \tag{11a}$$

$$\Lambda_r(\theta_s,\theta_r)=\frac{\mu_0}{g+\delta(\theta_s,\theta_r)} \tag{11b}$$

where μ_0 is the vacuum permeability, g is the air-gap length, θ_r and θ_s are rotor position and angular position in the air gap. $\delta(\theta_s)$ denotes the equivalent air-gap length due to the fact that additional air gap is introduced by stator slotting, which can be further expressed as [22]

$$\delta(\theta_s)=a_0+\sum_{n=1}^{+\infty}a_n\cos(nN_s\theta_s)+b_n\sin(nN_s\theta_s) \tag{12}$$

where the coefficients a_0, a_n, and b_n can be expressed as [22]

$$a_0=\frac{R_{iso}(\pi\beta_s)^2}{6N_s} \tag{13}$$

$$a_n=-\frac{R_{iso}}{2N_sn^2}\left\{\left(1+\cos(2\pi\beta_s)\right)-\frac{1}{\pi n\beta_s}\sin(2\pi n\beta_s)\right\} \tag{14}$$

$$b_n=\frac{R_{iso}}{2N_sn^2}\left\{\frac{1}{\pi n\beta_s}\left(1-\cos(2\pi\beta_s)\right)-\sin(2\pi n\beta_s)\right\} \tag{15}$$

where β_s is stator slot opening ratio that refers to the ratio of slot opening width to slot pitch. N_s is the stator slot number, R_{iso} is the stator inner radius. Analogously, the same procedure is applied to the rotor slots, and the corresponding air-gap permeance $\delta(\theta_s, \theta_r)$ due to the rotor slotting can be given by

$$\delta(\theta_s,\theta_r)=a_0'+\sum_{n=1}^{+\infty}a_n'\cos(nN_s(\theta_s-\theta_r))+b_n'\sin(nN_s(\theta_s-\theta_r)) \tag{16}$$

$$a_0'=\frac{R_{ro}(\pi\beta_r)^2}{6N_r} \tag{17}$$

$$a_n'=-\frac{R_{ro}}{2N_rn^2}\left\{\left(1+\cos(2\pi\beta_r)\right)-\frac{1}{\pi n\beta_s}\sin(2\pi n\beta_r)\right\} \tag{18}$$

$$b_n'=\frac{R_{ro}}{2N_sn^2}\left\{\frac{1}{\pi n\beta_r}\left(1-\cos(2\pi\beta_r)\right)-\sin(2\pi n\beta_r)\right\} \tag{19}$$

where β_r is rotor slot opening ratio, N_r is the rotor pole number, R_{ro} is the rotor outer radius. The inner air-gap permeance $\Lambda(\theta_s, \theta_r)$ can be approximately calculated by accounting for the inner stator/rotor doubly saliency, i.e.,

$$\Lambda(\theta_s,\theta_r)=\frac{2}{g}\left[\frac{\Lambda_s(\theta_s)\Lambda_r(\theta_s,\theta_r)}{\Lambda_s(\theta_s)+\Lambda_r(\theta_s,\theta_r)}\right] \tag{20}$$

3) Air-Gap Flux Density

The inner air-gap flux density $B_{ri}(\theta_s, \theta_r)$ can be considered as the resultant effects by the PM MMF and the inner stator/rotor pole modulation, which can be expressed as

$$B_{ri}(\theta_s,\theta_r)=\Lambda_r(\theta_s,\theta_r)\times F_m \tag{21}$$

In this case, it can be assumed that the air-gap fluxes perpendicularly entry the rotor pole surface by neglecting the rotor pole flux leakage and localized magnetic saturation. As a result, the outer rotor surface flux density $B_{iron}(\theta_s, \theta_r)$ can be treated as an integration of the air-gap field over one rotor pole pitch [23], i.e.,

$$B_{\text{iron}}(\theta_s,\theta_r)=\gamma_r\int_{(i-1)\theta_s}^{i\theta_s}B_{ri}(\theta_s,\theta_r)d\theta_s \tag{22}$$

where γ_r is the rotor pole flux concentration coefficient defined by [23]

$$\gamma_r=\frac{R_{ro}+g/2}{R_{ro}\tau(1-\beta_s)} \tag{23}$$

Consequently, the outer air-gap flux density $B_{ro}(\theta_s, \theta_r)$ can be calculated by introducing the slotted air-gap permeance Λ_{rel}, such as

$$B_{ro}(\theta_s,\theta_r)=\Lambda_{rel}\times B_{\text{iron}}(\theta_s,\theta_r) \tag{24}$$

with

$$\Lambda_{rel}=\frac{g\mu_0}{\mu_0[g+\Gamma(\theta_s)]} \tag{25}$$

where the resultant length of the flux paths in the outer stator opening can be expressed as

$$\Gamma(\theta_s)=\frac{\pi R_{osi}}{2}\frac{\sin\left(\frac{\theta_s}{2}\right)\sin\left(\frac{b_0}{2}-\frac{\theta_s}{2}\right)}{\sin\left(\frac{b_0}{4}\right)\sin\left(\frac{\theta_s}{2}-\frac{b_0}{4}\right)} \tag{26}$$

where R_{osi} is the inner radius of the inner stator, b_0 is the outer stator slot opening.

The analytically and FE predicted open-circuit inner and outer air-gap flux density waveforms are plotted in Fig. 6. Basically, the analytical results agree satisfactorily with the FE predictions, despite the discrepancy of the localized flux loci due to the fact that the localized magnetic saturation and flux leakage are neglected in the analytical method.

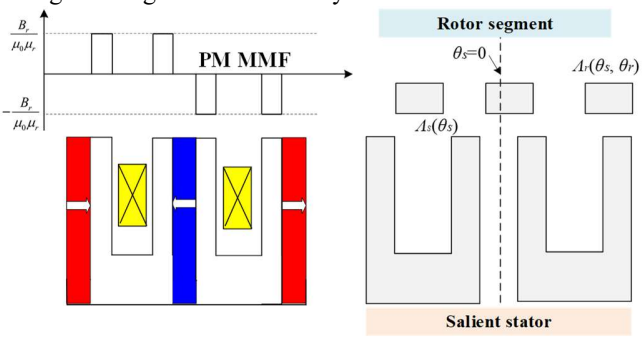

Fig. 5. Simplified permeance model of the proposed DS-BPMM.

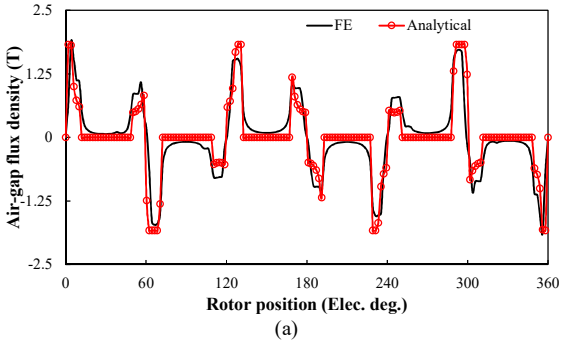

(a)

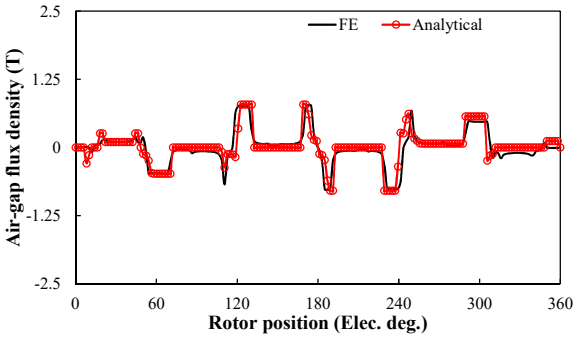

(b)

Fig. 6. Comparison of the FE and analytically predicted air-gap flux density waveforms. (a) Inner air-gap. (b) Outer air-gap.

The phase back-EMFs of the inner and outer windings can be further expressed as

$$E_{iph}(\theta_s) = -\frac{d}{dt}\left((R_{osi} + g/2) L_a \int_0^{2\pi} B_{ri} N(\theta_s) d\theta_s \right) \quad (27)$$

$$E_{oph}(\theta_s) = -\frac{d}{dt}\left((R_{ro} + g/2) L_a \int_0^{2\pi} B_{ro} N(\theta_s) d\theta_s \right) \quad (28)$$

where the winding function $N(\theta_s)$ can be expressed as

$$N(\theta_s) = \sum_{i=1,3,5}^{\infty} \frac{2}{n\pi} \frac{N_s}{N_r} k_{wi} \cos(iN_r\theta_s) \quad (29)$$

where k_{wi} is the ith harmonic of the winding factor. As a result, the total electromagnetic torque equation T_e can be expressed as

$$T_e = \frac{\sum_{n=a,b,c} E_{ophn}(\theta_s) I_{on} + \sum_{n=a,b,c} E_{iphn}(\theta_s) I_{in}}{\omega_r} \quad (30)$$

For the electric loadings, the total outer and inner armature slot areas can be modelled as

For the outer stator:

$$A_{so} = \pi \left[\left(\frac{D_{sb2}}{4} + \frac{D_{g2}}{4} - \frac{D_{g2}\beta_s}{2} \right) \left(D_{sb2} - D_{g2} \right) \right] \quad (31)$$

For the inner stator

$$A_{si} = \frac{1}{4}\pi \left(D_{g1}^{\ 2} - D_{sb1}^{\ 2} \right) - 15\tau_m \left(D_{g1} - D_{sb1} \right) \quad (32)$$

where D_{sb2} is the outer stator back iron diameter. D_{sb1} is the inner stator back iron diameter, and τ_m can be given by

$$\tau_m = \frac{\pi D_{g1}}{12} \frac{\beta_{ms}}{1 + 1/\beta_{ms}} \quad (33)$$

Since the inner stator employs parallel tooth configurations, the following equation should satisfy

$$\frac{D_{sb1}}{D_{g1}} = \frac{1.5\tau_m}{1.5\tau_m + 0.5\tau_{so}} \quad (34)$$

B. Optimization of the Key Parameters

1) Selection of the Rotor Pole Number

For the DS-BPMM having 6 stator slots, the normalized torque as a function of the rotor segment number N_r is plotted in Fig. 7. Obviously, the 6-stator slot machine model having 11-rotor pole, which exhibits highest torque capability, will be selected for the following analyses.

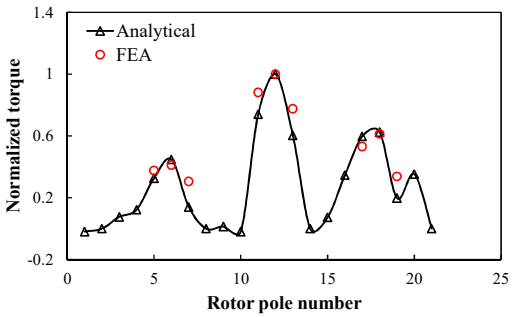

Fig. 7. Variation of normalized torque with number of rotor pole number in 6-stator pole DS-BPMM.

2) Optimal Combination of Effective Split Ratio and PM Loading Ratio

Therefore, the variation of normalized torque with λ_s and β_{ms} is calculated by the analytical model and FE method as shown in Fig. 8. It can be seen that the analytically predicted optimal points match well with the FE predictions. The torque basically increases with the magnet thickness when the split ratio is small due to the dominant contribution of the outer armature winding on the power output. Whereas, the optimum magnet thickness decreases with increasing the effective split ratio since the inner stator armature winding dominants the torque production. As a result, the torque maximizes when λ_s and β_{ms} approximately equal 0.67 and 0.22, respectively. Consequently, the optimal power splitting ratio is obtained, i.e. 1.31, which implies that the torque production is mainly contributed by the outer armature windings due to the larger copper areas of the outer stator.

3) Optimization of the Electric Loading Splitting Ratio

The splitting ratio between two stator armature copper losses is another important issue for the torque improvement. FE and analytical methods are carried out to calculate the average torque as a function of the copper loss ratio of the outer armature winding to the total one, as shown in Fig. 9. It can be seen that the analytically predicted results agree well with the FEA ones, when the optimal copper loss ratio is approximately 0.75. This is mainly attributed to the higher armature turns in the outer stator. The mismatch between the two results are resulted by the fact that the analytical method ignores nonlinear magnetic saturation, leakage flux and end effect, etc.

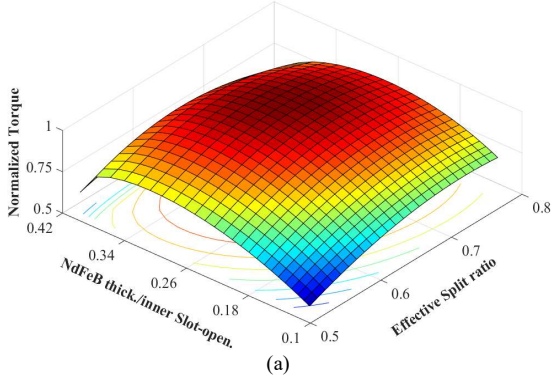

(a)

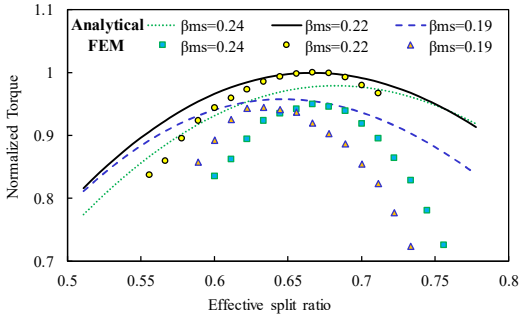

(b)

Fig. 8. Variations of normalized torque with λ_s and β_{ms}. (a) Analytical results. (b) Comparison between analytical- and FE-predictions.

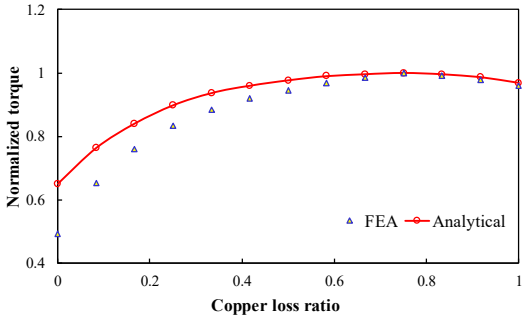

Fig. 9. Comparison of analytical and FEA predictions of the normalized torque variation with the copper loss ratio.

IV. Electromagnetic Performance Comparison of the Proposed DS-BPMM and Existing DS Counterparts

In order to highlight the advantages of the proposed DS-BPMM particularly in terms of the torque improvement with PM usage reduction, the electromagnetic characteristics of the proposed machine are investigated and compared with the existing DS-SFPM machines with two similar stators as above-mentioned in [14] and [15]. The DS machines having rotor back-iron is termed as model I, while the yokeless DS machine is referred as model II. It should be noted that in the yokeless conventional machines, the PMs located on two separate stators are magnetized in opposite direction, and hence the PM magnetic flux reverses its direction of flow over half an electric cycle so as to comply with the SF operating principle. On the other hand, the PMs in the model I are with the same magnetization direction, which can avoid the magnetic circuit coupling between two stators. Overall, the three machines are designed with the same stator slot/rotor pole numbers, overall dimensions, armature winding turns and the same constraint total copper loss of 60W for fair comparison. The optimized major design parameters are listed in Table I.

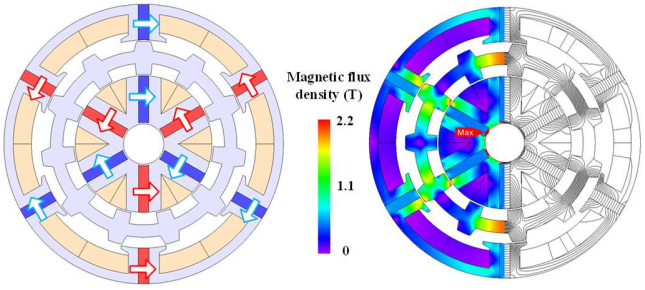

(a)

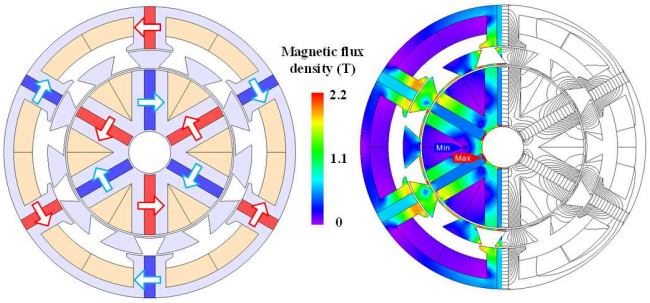

(b)

Fig. 10. The topologies and open-circuit field distributions of the conventional DS machines. (a) Model I. (b) Model II.

A. Open-Circuit Back-EMF

The topologies and open-circuit field distributions of the investigated DS machines are shown in Fig. 10. It can be observed that the conventional yokeless DS machine suffers from significant magnetic saturation particularly in the outer stator, which is resulted by the series magnetic circuits between two PMs located on the two stators. Meanwhile, negligible magnetic coupling can be observed in the two stator PM excitations in model I due to the parallel magnetic circuit relationship. Fig. 11 illustrates the open-circuit back-EMFs of the three investigated machines at 400 r/min. It can be observed that model-I exhibits comparable EMF with model-II, but both lower than proposed DS-BPMM. This is mainly attributed to larger outer armature slot in DS-BPMM and the severe magnetic saturation occurring in the conventional DS machines, as reflected in Fig. 10.

TABLE I
Key Design Parameters of DS-BPMM and Conventional DS Machines

Items	DS-BPMM	Model-I	Model-II
Outer diameter of outer stator (mm),D_{so}		90	
Inner diameter of outer stator (mm), D_{si}	79	64	67
Back-iron thickness (mm), h_{bi}		3	
Outer stator tooth arc (deg.), b_{st}	20	14	23
Outer stator tooth-tip width (mm), b_{st}	11.6	12	10
Air-gap length (mm), g_i, g_o		0.5	
Arc of outer rotor edge (deg.), l_{r1}	12	25	13
Arc of inner rotor edge (deg.), l_{r2}	25	12	14
Rotor segment thickness (mm), h_r	4.5	5.5	7
Active stack length (mm), l_{ef}		25	
Inner NdFeB thickness×length (mm)	-	3.3×15	3.3×13
Inner NdFeB thickness×length (mm)	3.3×22	3.3×11	2×18
Rated speed (r/min)		400	
PM volume (cm^3)	10.89	12.87	11.835
NdFeB PM grade		N35SH	
Rated total copper loss (W)		60	
Number of outer armature turns per coil		84	
Number of inner armature turns per coil		72	

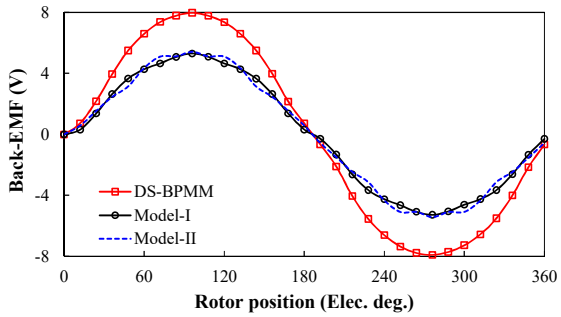

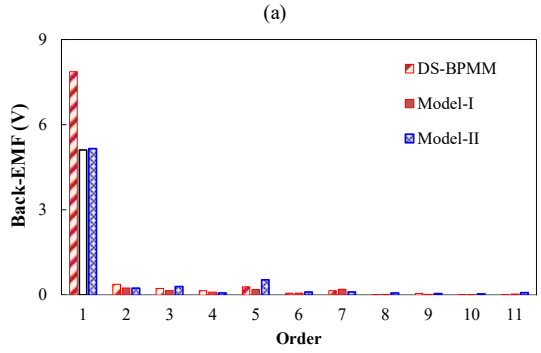

(a)

(b)

Fig. 11. The open-circuit back-EMFs of the DS machines. (a) Waveforms. (b) Harmonic spectra.

B. Torque Characteristics

In order to choose an appropriate maximum-torque-per-ampere (MPTA) control strategy, the torque-current angle characteristics are firstly investigated as shown in Fig. 12(a). It can be observed that all the three machines exhibit negligible saliency ratio. Thus, the zero *d*-axis current control is selected to maximize the torque in these cases. Besides, the steady-state torque waveforms under rated current (I_{rms}=15A, "rms" denotes root-mean-square value) and zero *d*-axis current control are shown in Fig. 12(b), in which the results agree well with those back-EMF results owing to the negligible reluctance torque. Due to larger outer armature slot areas and less magnetic saturation, the DS-BPMM exhibits 44.2% higher torque than mode-I and II with less magnet usage.

C. Iron Loss Evaluation

The iron loss density distributions of the three models under rated-load operation are plotted in Fig. 13. It can be seen that the majority of iron losses can be observed in the rotor segments. Meanwhile, the iron loss distribution of the outer stator differ significantly with those conventional counterparts. Moreover, the iron losses in each components are listed in Table II. It shows that model-I suffers from highest iron loss, which is mainly attributed to its dominantly high rotor loss. The significant magnetic saturation in the rotor segments of model-I is responsible for this phenomenon. In addition, the iron loss of the proposed design exceeds model-II due to its high outer stator core loss.

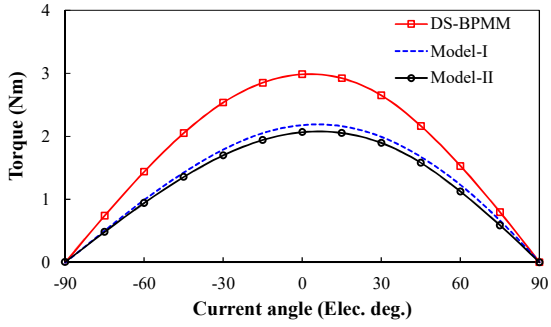

(a)

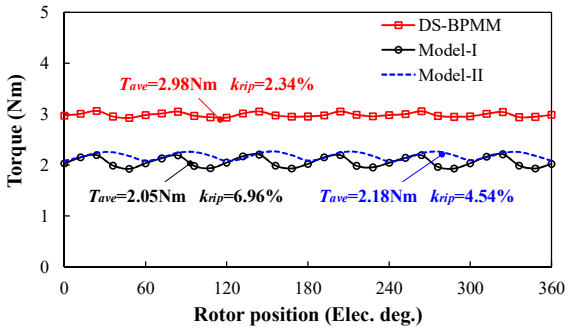

(b)

Fig. 12. Comparison of torque characteristics of the DS machines. (a) Torque-current angle characteristics. (b) Steady-torque waveforms. (Rated current=10Arms)

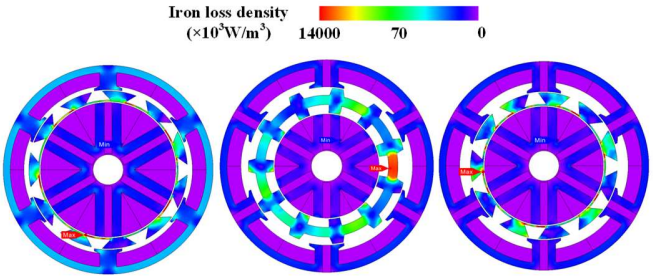

(a) (b) (c)

Fig. 13. The iron loss distributions of the three DS machines. (a) Proposed DS-BPMM. (b) Model-I. (c) Model-II.

D. Demagnetization Withstand Capability

The demagnetization capability subject to severe armature reaction should be examined to permit the expected on-load torque capability. The PM demagnetization risk is increased at high operating temperatures due to the nonlinear *B–H* characteristics of the magnet. The PM field distributions subject to temperature 120 °C and *q*-axis current of 25A are shown in Fig. 14. It can be observed that model II exhibits best demagnetization risk withstand capability. The fact that the series magnetic circuit relationship between the two stators is responsible for higher PM working points in model-II.

TABLE II
IRON LOSS CHARACTERISTICS OF DS-BPMM AND CONVENTIONAL DS MACHINES

Iron loss	DS-BPMM	Model-I	Model-II
Outer stator	0.98	0.51	0.46
Inner stator	0.40	0.16	0.23
Rotor	0.23	1.18	0.63
Total	1.61	1.85	1.32

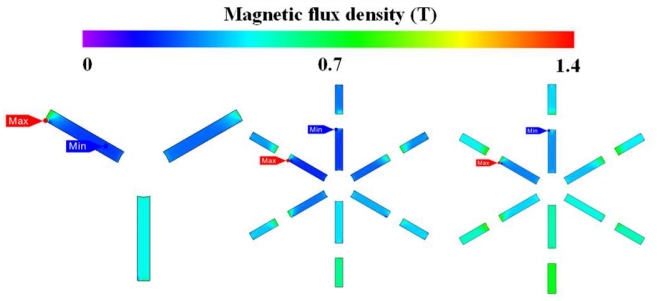

(a) (b) (c)

Fig. 14. The PM working point distributions. (a) Proposed DS-BPMM. (b) Model-I. (c) Model-II.

Fig. 15. The DS-BPMM prototype. (a) Inner stator assemblies. (b) Rotor assembly. (c) Outer stator.

E. Comparison with Transverse-Flux Machines

Since the switched flux pattern and operating principle of the proposed DS-BPMM is similar to that of the PM transverse-flux machine (PMTF) machine reported in [24]-[27], the advantages and disadvantages of the proposed DS-BPMM and the three-phase TFM [24] are discussed and compared in this part. The key electromagnetic characteristics of the proposed DS machine and PMTF machine at the same current density are compared and tabulated in Table III. It shows that the power density, power factor, efficiency and torque-to-magnet-volume of the proposed machine are higher than those of the PMTF. Meanwhile, the torque ripple issue of the PMTF machine appears to be more severe, which is mainly attributed to the flux leakage and relatively low PM utilization ratio in the PMTF machine. However, the PMTF machine has higher power-to-weight ratio due to its compact assembly. Moreover, the decoupling of phases, easy winding wrapping and the stator modularization make the PMTF machine attractive for fault-tolerant safety-critical applications [26].

From the viewpoint of manufacturing, the rotor assembly with a cantilever structure and PM installing of the proposed DS-BPMM are relatively more complicated than that of the PMTF machine. The requirement of the aluminum housing for fixing the stator modules appears to be more challenging than the stator manufacturing of the proposed DS-BPMM.

Specifically, the outer stator of the proposed DS-BPMM is similar to that of the conventional fractional-slot machine, which is easy to manufacture. On the other hand, since the sandwiched rotor is a cantilever structure, the mechanical aspect should be considered. The rotor ribs are employed to connect the rotor iron pieces in order to facilitate the manufacturing. Meanwhile, the rotor iron pieces are encapsulated in epoxy resin. The metallic sticks are embedded in the epoxy resin, and are linked with the end caps for fixation. It should be noted that the epoxy resin can provide certain mechanical strength since the tensile strength is 85N/mm². Hence, the prototype is able to tolerate certain severe working conditions [18]. Nonetheless, for the high power-rating cases, it is critical to cope with mechanical issues. Another alternate solution such as the aluminum alloy reinforcement or carbon-fiber bandage can be employed.

On the other hand, for the PMTF machine, PMs are placed in the specially cut grooving on the rotor inner and outer surface, and the magnetic outer poles are connected to the stator core with the aid of metallic ties [24]. In addition, the machine housing can also be made of aluminum, which may bring eddy-current issue [24]. Another challenge for manufacturing is high torque ripple and induced vibration issue, the magnetic shunts are reported to minimize this problem [25], but the cost and power-to-weight ratio would be decreased.

TABLE III
COMPARISON OF DS-BPMM AND PMTF MACHINE

Items	Unit	DS-BPMM	PMTF [23]
Current density	A/mm^2	4.5	
Power density	kW/m^3	476	140
Torque ripple	%	2.34	12.00
Cogging torque/rated torque	%	2.68	53.33
Power to weight ratio	kW/kg	0.03	0.05
Torque/magnet volume	Nm/L	292.10	133.17
Power factor	-	0.89	0.85
Efficiency @rated load/speed	%	90.8	90.0

V. EXPERIMENTAL VALIDATION

In order to experimentally verify the aforementioned analyses, an optimized 6/11-stator slot/rotor pole DS-BPMM prototype is manufactured and tested. The stator and rotor assemblies are shown in Fig. 15. The mechanical aspects on this type of machine have been discussed in [18].

Under the 400r/min, the measured open-circuit phase back-EMFs are compared with FE results as shown in Fig. 16. In addition, the torque against current characteristics under zero *d*-axis current control are compared in Fig. 17. The fact that the mechanical tolerances and end-effect are not included in the FE analyses results in the slight mismatch between FE predicted and measured results. Overall, the satisfactory agreement between FE and measured results has confirmed the feasibility of the proposed design.

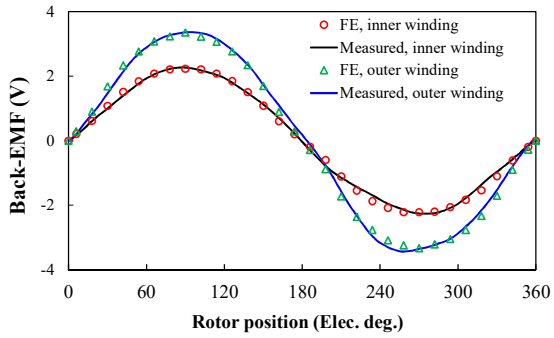

Fig. 16. FE-predicted and measured open-circuit phase Back-EMFs.

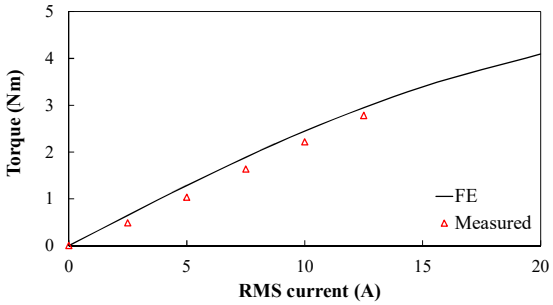

Fig. 17. FE-predicted and measured torque-current characteristics.

VI. CONCLUSIONS

In this paper, a novel DS-BPMM only having PM excitations in the inner stator is proposed, which can be considered as a

synergy of an outer-rotor stator PM machine combined with a separate outer stator. With the proposed design, the space tradeoff between PM and copper areas and severe magnetic saturation are significantly alleviated compared to the traditional DS counterparts. An optimized prototype is manufactured and tested to verify the FE analyses. The key findings can be summarized as follows.

1) The proposed DS design can be derived from a traditional PS one, and approximately 36.6% torque improvement at rated load can be obtained with another set of armature winding in the inner stator.
2) The stator slot/rotor pole combination and power splitting ratio between two stators are analytically optimized by simplified air-gap permeance model. It shows that the highest torque capability can be obtained in the 6/11-pole configuration. Besides, the optimal copper loss ratio between two stators is ~0.75, which can achieve the torque maximization with constraint total copper loss.
3) The electromagnetic characteristics of the proposed DS-BPMM and conventional DS structures are evaluated and compared. It shows that the proposed design exhibits 44.2% higher rated-load torque than model-I and II with less magnet usage. Meanwhile, the lowest iron loss and the best demagnetization withstand capability can be observed in model-II.

REFERENCES

[1] G. A. Capolino and A. Cavagnino, "New trends in electrical machines technology," *IEEE Trans. Ind. Electron*., vol. 61, no. 8, pp. 4281–4285, Aug. 2014.

[2] K. T. Chau, Electric vehicle machines and drives–design, analysis and application. New York, NY, USA: Wiley, 2015.

[3] Z. Q. Zhu and D. Howe, "Electrical machines and drives for electric, hybrid, and fuel cell vehicles," *Proc. IEEE*, vol. 95, no. 4, pp. 746-765, Apr. 2007.

[4] Cheng M, Han P, Buja G, and Jovanović, M. G. "Emerging multi-port electrical machines and systems: past developments, current challenges and future prospects," *IEEE Trans. Ind. Electron.*, in press.

[5] J. Bai, P. Zheng, C. Tong, Z. Song, and Q. Zhao, "Characteristic analysis and verification of the magnetic-field modulated brushless double-rotor machine," *IEEE Trans. Ind. Electron*., vol. 62, no. 7, pp. 4023-4033, Jul. 2015.

[6] M. Abbasian, M. Moallem, and B. Fahimi, "Double-stator switched reluctance machines (DSSRM): fundamentals and magnetic force analysis," *IEEE Trans. Energy Convers*., vol. 25, no. 3, pp. 589-597, Sep. 2010.

[7] Y. B. Wang, M. Cheng, Y. Du, and K. T. Chau, "Design of high-torque density double-stator permanent magnet brushless motors," *IET Electr. Power Appl*., vol. 5, no. 3, pp. 317-323, Mar. 2011.

[8] W. Zhao, D. Xu, T. A. Lipo, and B. Kwon, "Dual airgap stator- and rotor-permanent magnet machines with spoke-type configurations using phase-group concentrated-coil windings," *IEEE Trans. Ind. Appl.*, in press.

[9] D. Li, R. Qu, and T. A. Lipo, "High power factor vernier permanent magnet machines," *IEEE Trans. Ind. Appl.*, vol. 50, no. 6, pp. 3664-3674, Nov./Dec. 2014.

[10] S. Niu, K. T. Chau, J. Z. Jiang, and C. Liu, "Design and control of a new double-stator cup-rotor permanent-magnet machine for wind power generation," *IEEE Trans. Magn*., vol. 43, no. 6, pp.2501-2503, June 2007.

[11] C. Liu, K.T. Chau, and Z. Zhang, "Novel design of double-stator single-rotor magnetic-geared machines," *IEEE Trans. Magn.*, vol. 48, no. 11, pp. 4180-4183, Oct. 2012.

[12] Y. Gao, R. Qu, D. Li, H. Fang, J. Li, and W. Kong, "A novel dual-stator Vernier permanent magnet machine," *IEEE Trans. Magn*., 2017, vol. 53, no. 11, pp: 1-5, Art. No. 8110105, Apr. 2017.

[13] Z. Y. Zong, L. Quan, and Y. M. Ge, "A new double-stator flux-switching permanent magnet machine for electric vehicle application," in *Rec. of IEEE Inter. Magn. Conf*., Dresden, Germany, 2014, pp. GP-5.

[14] L. Zhou, W. Hua, and M. Chen, "A novel co-axial dual flux-switching permanent magnet machine for hybrid electric vehicles," Dresden, Germany, 2014, pp. 1-1.

[15] C. C. Awah and Z. Q. Zhu, "Comparative study of high performance double stator switched flux permanent magnet machines," in *Proc VPPC 2016*, IEEE, pp. 1-6.

[16] D. Kim, H. Hwang, S. Bae and C. Lee, "Analysis and design of double stator flux-switching permanent magnet machine using ferrite magnet in hybrid electric vehicles, *IEEE Trans. Magn*., vol. PP, no. 99, pp. 1-4, 2016.

[17] D. Evans and Z. Q. Zhu, "Novel partitioned stator switched flux permanent magnet machines," *IEEE Trans. Magn*., vol. 51, no. 1, Art. no. 8100114, Jan. 2015.

[18] H. Hua, Z.Q. Zhu, C. Wang, M. Zheng, Z. Z. Wu, D. Wu, and X. Ge, "Partitioned stator machines with NdFeB and ferrite magnets," *IEEE Trans. Ind. Appl.*, vol.53, no.3, pp.1870-1882, Jan. 2016.

[19] H. Yang, Z. Q. Zhu, H. Lin, Y. Zhang, S. Fang, Y. Huang, and N. Feng, "Performance improvement of partitioned stator switched flux memory machines with triple-magnet configuration," *IEEE Trans. Magn.*, vol. 52, no. 7, Article. 8104604, Jul. 2016.

[20] T. Sheng and S. Niu, "Design of doubly complementary stator-PM machine with high magnet utilization factor for low cost applications," *IEEE Trans. Energy Convers.*, vol. 33, no. 2, pp. 567-575, Jun. 2018.

[21] D. Li, R. Qu, J. Li, W. Xu, and L. Wu, "Synthesis of flux switching permanent magnet machines," *IEEE Trans. Energy Convers.* vol. 31, no. 1, pp. 106-117, Mar. 2016.

[22] B. Gaussens, E. Hoang, O. De la Barriere, J. Saint-Michel, M. Lecrivain, and M. Gabsi, "Analytical approach for air-gap modeling of field- excited flux-switching machine: no-load operation," *IEEE Trans. Magn*., vol. 48, no. 9, pp. 2505-2517, Sep. 2012.

[23] B. Gaussens, E. Hoang, O. De la Barriere, J. Saint-Michel, P. Manfe, M. Lecrivain, and M. Gabsi, "Uni- and bidirectional flux variation loci method for analytical prediction of iron losses in doubly-salient field-excited switched-flux machines," *IEEE Trans. Magn*., vol. 49, no. 7, pp. 4100-4103, Jul. 2013.

[24] O. Dobzhanskyi and R. Gouws, "Performance analysis of a permanent magnet transverse flux generator with double coil," *IEEE Trans. Magn*., vol. 52, no. 1, Art. No. 8200111, Jan. 2016.

[25] O. Dobzhanskyi, R. Gouws, and E. Amiri, "On the role of magnetic shunts for increasing performance of transverse flux machines," *IEEE Trans. Magn*., vol. 53, no. 2, Art. No. 8100808, Feb. 2017.

[26] O. Dobzhanskyi, R. Gouws, and E. Amiri, "Analysis of PM transverse-flux outer rotor machines with different configuration," *IEEE Trans. Ind. Appl.*, vol. 53, no. 5, pp. 4260-4268, Sept./Oct. 2017.

[27] O. Dobzhanskyi, R. Gouws, and E. Amiri, "Comparison analysis of PM transverse flux outer rotor machines with and without magnetic shunts," in *Proc. ECCE 2016*, IEEE, pp. 1-8.